

Dimension constraints improve hypothesis testing for large-scale, graph-associated, brain-image data

TIEN VO, VAMSI ITHAPU, VIKAS SINGH,
MICHAEL A. NEWTON*

*Department of Biostatistics and Medical Informatics, University of Wisconsin at Madison 610 Walnut
Street, Madison, WI USA
newton@biostat.wisc.edu*

SUMMARY

For large-scale testing with graph-associated data, we present an empirical Bayes mixture technique to score local false-discovery rates. Compared to procedures that ignore the graph, the proposed GraphMM method gains power in settings where non-null cases form connected sub-graphs, and it does so by regularizing parameter contrasts between testing units. Simulations show that GraphMM controls the false-discovery rate in a variety of settings. On magnetic resonance imaging data from a study of brain changes associated with the onset of Alzheimer’s disease, GraphMM produces substantially greater yield than conventional large-scale testing procedures.

Key words: empirical Bayes, graph-respecting partition, GraphMM, image analysis, local false-discovery rate, mixture model

*To whom correspondence should be addressed.

1. INTRODUCTION

Empirical Bayesian methods provide a useful approach to large-scale hypothesis testing in genomics, brain-imaging, and other application areas. Often, these methods are applied relatively late in the data-analysis pipeline, after p-values, test statistics, or other summary statistics are computed for each testing unit. Essentially, the analyst performs univariate testing *en masse*, with the final unit-specific scores and discoveries dependent upon the chosen empirical Bayesian method, which accounts for the collective properties of the separate statistics to gain an advantage (e.g., Storey (2003), Efron (2010), Stephens (2017)). These methods are effective but may be underpowered in some applied problems when the underlying effects are relatively weak. Motivated by tasks in neuroscience, we describe an empirical Bayesian approach that operates earlier in the data-analysis pipeline and that leverages regularities achieved by constraining the dimension of the parameter space. Our approach is restricted to data sets in which the variables constitute nodes of a known, undirected graph, which we use to guide regularization. We report simulation and empirical studies with structural magnetic resonance imaging to demonstrate the striking operating characteristics of the new methodology. We conjecture that power is gained for graph-associated data by moving upstream in the data reduction process and by recognizing low complexity parameter states.

The following toy problem illustrates in a highly simplified setting the phenomenon we leverage for improved power. Suppose we have two sampling conditions, and two variables measured in each condition, say X_1 and X_2 in the first condition and Y_1 and Y_2 in the second. We aim to test the null hypothesis that X_1 and Y_1 have the same expected value; say $H_0 : \mu_{X_1} = \mu_{Y_1}$. Conditional upon target values μ_{X_1} , μ_{Y_1} and nuisance mean values μ_{X_2} and μ_{Y_2} , the four observations are mutually independent, with normal distributions and some constant, known variance σ^2 . We further imagine that these four variables are part of a larger system, throughout which the distinct expected values themselves fluctuate, say according to a standard normal

distribution. Within this structure, a test of H_0 may be based upon the local false-discovery rate

$$\text{lfdr}_1 = P(H_0|X_1, Y_1) = \frac{p_0 f(X_1, Y_1)}{p_0 f(X_1, Y_1) + (1 - p_0)g(X_1)g(Y_1)}$$

where we are mixing discretely over null (with probability p_0) and non-null cases. Notice in this setting the across-system variation in expected values may be handled analytically and integrated out; thus in this predictive distribution g is the density of a mean 0 normal distribution with variance $1 + \sigma^2$; and f is the bivariate normal density with margins g and with correlation $1/(1 + \sigma^2)$ between X_1 and Y_1 . In considering data X_2 and Y_2 on the second variable, it may be useful to suppose that the expected values here are no different from their counterparts on the first variable. We say the variables are blocked if both $\mu_{X_1} = \mu_{X_2}$ and $\mu_{Y_1} = \mu_{Y_2}$, and we consider this a discrete possibility that occurs with probability p_{block} throughout the system, independently of H_0 . In the absence of blocking there is no information in X_2 and Y_2 that could inform the test of H_0 (considering the independence assumptions). In the presence of blocking, however, data on these second variables are highly relevant. Treating blocking as random variable across the system, we would score H_0 using the local false-discovery rate $\text{lfdr}_2 = P(H_0|X_1, X_2, Y_1, Y_2)$, which requires consideration of a 4-variate normal and joint discrete mixing over the blocking and null states for full evaluation. Fig. 1 shows the result of simulating a system with 10^4 variable pairs, where the marginal null frequency $p_0 = 0.8$, $\sigma^2 = 1/2$, and the blocking rate p_{block} varies over three possibilities. Shown is the false-discovery rate of the list formed by ranking instances by either lfdr_1 or lfdr_2 . The finding in this toy problem is that power for detecting differences between μ_{X_1} and μ_{Y_1} increases by accounting for the blocking, since the list of discovered non-null cases by lfdr_2 is larger for a given false-discovery rate than the list constructed using lfdr_1 . In other words, when the dimension of the parameter space is constrained, more data become relevant to the test of H_0 and power increases.

Our interest in large-scale testing arises from work with structural magnetic resonance imaging (sMRI) data measured in studies of brain structure and function, as part of the

Alzheimer's Disease Neuroimaging Initiative (ADNI-2) (Weiner and Veitch (2015)). sMRI provides a detailed view of brain atrophy and has become an integral to the clinical assessment of patients suspected to have Alzheimer's disease (AD) (e.g., Vemuri and Jack (2010), Moller *and others* (2013)). In studies to understand disease onset, a central task has been to identify brain regions that exhibit statistically significant differences between various clinical groups, while accounting for technical and biological sources of variation affecting sMRI scans. Existing work in large-scale testing for neuroimaging has considered thresholds on voxel-wise test statistics to control a specified false positive rate and maintain testing power (Nichols (2012)). Two widely used approaches are family-wise error control using random field theory (e.g., Worsley *and others* (2004)) and false-discovery rate control using Benjamin-Hochberg procedure (e.g., Genovese *and others* (2002)). The former is based on additional assumptions about the spatial smoothness of the MRI signal which may be problematic (Eklund *and others* (2016)). Both parametric and nonparametric voxel-wise tests are available in convenient neuroimaging software systems (Penny *and others* (2007), Nichols). Recently Tansey *and others* (2018) presented an FDR tool that processes unit-specific test statistics in a way to spatially smooth the estimated prior proportions. As the clinical questions of interest move towards identifying early signs of AD, the changes in average brain profiles between conditions invariably become more subtle and increasingly hard to detect; the result is that very few voxels or brain regions may be detected as significantly different by standard methods.

Making a practical tool from the power boosting idea in Fig. 1 requires that a number of modeling and computational issues be resolved. Others have recognized the potential, and have designed computationally intensive Bayesian approaches based on Markov chain Monte Carlo (Do *and others* (2005), Dahl and Newton (2007), Dahl *and others* (2008), Kim *and others* (2009)). We seek simpler methodology that may be more readily adapted in various applications. In many contexts data may be organized at nodes of an undirected graph, which

will provide a basis for generalizing the concept of blocking using graph-respecting partitions that have a regularizing effect. Having replicate observations per group is a basic aspect of the data structure, but we must also account for statistical dependence among variables for effective methodology. In the proposed formulation we avoid the product-partition assumption that would greatly simplify computations but at the expense of model validity and robustness; we gain numerical efficiency and avoid posterior Markov chain Monte Carlo through a graph-localization of the mixture computations. The resulting tool we call GraphMM, for graph-based mixture model. It is deployed as a freely available open-source R package available at <https://github.com/tienv/GraphMM/>. We investigate its properties using a variety of synthetic-data scenarios, and we also apply it to identify statistically significant changes in brain structure associated with the onset of mild cognitive impairment. Details not found in the following sections are included in Supplementary Material.

2. METHODS

2.1 Data structure and inference problem

Let $G = (V, E)$ denote a simple, connected, undirected graph with vertex set $V = \{1, 2, \dots, N\}$ and edge set E , and consider partitions of V , such as $\Psi = \{b_1, \dots, b_K\}$; that is, blocks (also called clusters) b_k constitute non-empty disjoint subsets of V for which $\cup_{k=1}^K b_k = V$. In the application in Section 3.2, vertices correspond to voxels at which brain-image data are measured, edges connect spatially neighboring voxels, and the partition conveys a dimension-reducing constraint. The framework is quite general and includes, for example, interesting problems from genomics and molecular biology. Recall that for any subset $b \subset V$, the induced subgraph $G_b = (b, E_b)$, where E_b contains all edges $e = (v_1, v_2)$ for which $e \in E$ and $v_1, v_2 \in b$. For use in constraining a parameter space, we introduce the following property:

Property 2.1 (Graph respecting partition) A partition Ψ respects G , or Ψ is graph-respecting, if for all $b_k \in \Psi$, the induced graph G_{b_k} is connected.

Fig. 2 presents a simple illustration; a spanning-tree representation turns out to be useful in computations (Supplementary Material). It becomes relevant to statistical modeling that the size of the set of graph-respecting partitions, though large, still is substantially smaller than the set of all partitions as the graph itself becomes less complex. For example there are 21147 partitions of $N = 9$ objects (the 9th Bell number), but if these 9 objects are arranged as vertices of a regular 3×3 lattice graph, then there are only 1434 graph-respecting partitions.

In our setting, the graph G serves as a known object that provides structure to a data set being analyzed for the purpose of a two-group comparison. This is in contrast, for example, to graphical-modeling settings where the possibly unknown graph holds the dependency patterns of the joint distribution. We write the two-group data as $\mathbf{X} = (X_{v,m})$ and $\mathbf{Y} = (Y_{v,r})$, where $v \in V$, $m = 1, \dots, M_X$ and $r = 1, \dots, M_Y$. Here M_X and M_Y denote the numbers of replicate samples in both groups. In Section 3.2, for example, m indexes the brain of a normal control subject and r indexes the brain of a subject with mild cognitive impairment. For convenience, let $\mathbf{X}_m = (X_{v,m}, v \in V)$ and $\mathbf{Y}_r = (Y_{v,r}, v \in V)$ denote the across-graph samples on subjects m and r , which we treat as identically distributed within group and mutually independent over m and r owing to the two-group, unpaired experimental design.

Our methodology tests for changes between the two groups in the expected-value vectors: $\boldsymbol{\mu}_X = E(\mathbf{X}_m) = (\mu_{X_1}, \dots, \mu_{X_N})$ and $\boldsymbol{\mu}_Y = E(\mathbf{Y}_r) = (\mu_{Y_1}, \dots, \mu_{Y_N})$. Specifically, we aim to test, for any vertex $v \in V$, $H_{0,v} : \mu_{X_v} = \mu_{Y_v}$ versus $H_{1,v} : \mu_{X_v} \neq \mu_{Y_v}$. We seek to gain statistical power over contemporary testing procedures by imposing a dimension constraint on the expected values. Although it is not required to be known or even estimated, we suppose there exists a

graph-respecting partition $\Psi = \{b_k\}$ that constrains the expected values:

$$\begin{cases} \mu_{X_v} = \mu_{X_u} & \text{if for some } k, \text{ both } v, u \in b_k \\ \mu_{X_v} \neq \mu_{X_u} & \text{if } v, u \text{ belong to different blocks} \end{cases} \quad (2.1)$$

$$\begin{cases} \mu_{Y_v} = \mu_{Y_u} & \text{if for some } k, \text{ both } v, u \in b_k \\ \mu_{Y_v} \neq \mu_{Y_u} & \text{if } v, u \text{ belong to different blocks} \end{cases}$$

All vertices v in block b_k have a common mean in the first group, say φ_k , and a common mean ν_k in the second group. The contrast on test, then, is $\delta_k = \nu_k - \varphi_k$; together with Ψ , the binary vector $\Delta = (\Delta_1, \dots, \Delta_K)$ holding indicators $\Delta_k = 1[\delta_k \neq 0]$ is equivalent to knowing whether or not $H_{0,v}$ is true for each vertex v . When data are consistent with a partition Ψ in which the number of blocks K is small compared to the number of vertices N , then it may be possible to leverage this reduced parameter-space complexity for the benefit of hypothesis-testing power.

2.2 Graph-based Mixture Model

2.2.1 *Discrete mixing.* We adopt an empirical Bayes, mixture-based testing approach, which requires that for each vertex we compute a local false-discovery rate:

$$l_v := P(H_{0,v} | \mathbf{X}, \mathbf{Y}) = \sum_{\Psi, \Delta} (1 - \Delta_k) \mathbb{1}(v \in b_k) P(\Delta, \Psi | \mathbf{X}, \mathbf{Y}). \quad (2.2)$$

Our list \mathcal{L} of discovered (non-null) vertices is $\mathcal{L} = \{v : l_v \leq c\}$ for some threshold c . Conditional on the data, the expected rate of type-I errors within \mathcal{L} is dominated by the threshold c (Efron (2007), Newton *and others* (2004)). The sum in (2.2) is over the finite set of pairs of partitions Ψ and block-change indicator vectors Δ . This set is intractably large for even moderate-sized graphs. We have experimented with Markov-chain Monte Carlo for general graphs, but present here exact computations in the context of very small graphs. Specifically, for each vertex v in the original graph we consider a small local subgraph in which v is one of the central vertices, and we simply deploy GraphMM on this local graph.

Summing in (2.2) delivers marginal posterior inference, and thus a mechanism for borrowing strength among vertices v . By Bayes's rule, $P(\Delta, \Psi | \mathbf{X}, \mathbf{Y}) \propto f(\mathbf{X}, \mathbf{Y} | \Delta, \Psi) P(\Delta, \Psi)$, and

both the mass $P(\Delta, \Psi)$ and the predictive density $f(\mathbf{X}, \mathbf{Y} | \Delta, \Psi)$ need to be specified to compute inference summaries. Various modeling approaches present themselves. For example, we could reduce data per vertex to a test statistic (e.g., t-statistic) and model the predictive density nonparametrically, as in the R package `locFDR` (see Efron (2010)). Alternatively, we could reduce data per vertex less severely, retaining effect estimates and estimated standard errors, as in adaptive shrinkage (Stephens (2017)). By contrast, we adopt an explicit parametric-model formulation for the predictive distribution of data given the discrete state (Ψ, Δ) . It restricts the sampling model to be Gaussian, but allows general covariance among vertices and is not reliant on the product-partition assumption commonly used in partition-based models (Barry and Hartigan (1992)). For $P(\Psi, \Delta)$, we specify $P(\Psi) \propto 1$, we encode independent and identically distributed block-specific Bernoulli(p_0) indicators in $P(\Delta | \Psi)$, and we use univariate empirical-Bayes techniques to estimate p_0 .

2.2.2 Predictive density given discrete structure. We take a multivariate Gaussian sampling model:

$$\mathbf{X}_m | \mu_X, U, \Psi, \Delta \sim_{\text{i.i.d.}} \mathcal{N}(\mu_X, U) \quad m = 1, \dots, M_X, \quad \mathbf{Y}_r | \mu_Y, W, \Psi, \Delta \sim_{\text{i.i.d.}} \mathcal{N}(\mu_Y, W) \quad r = 1, \dots, M_Y.$$

We do not constrain the $N \times N$ covariance matrices U and W , though we place a conjugate inverse Wishart prior distribution on them: $U | \Psi, \Delta, \mu_X, \mu_Y \sim \mathcal{IW}(A, \text{df})$, and $W | \Psi, \Delta, \mu_X, \mu_Y \sim \mathcal{IW}(B, \text{df})$. In general there is no simple conjugate reduction for predictive densities owing to the less-than-full dimension of free parameters in μ_X and μ_Y . On these free parameters we further specify independent Gaussian priors: $\varphi_k \sim \mathcal{N}(\mu_0, \tau^2)$ and, for $\Delta_k \neq 0$, $\delta_k \sim \mathcal{N}(\delta_0, \sigma^2)$. Hyperparameters in `GraphMM` include scalars $\delta_0, \mu_0, \tau^2, \sigma^2, \text{df}$, and matrices A, B , which we estimate from data across the whole graph following the empirical-Bayes approach.

The above specification induces a joint density $f(\mathbf{X}, \mathbf{Y}, \mu_X, \mu_Y, U, W | \Delta, \Psi)$. For the purpose of hypothesis testing, we need to marginalize most variables, since $H_{0,v}$ is equivalent to $\Delta_k = 0$ and $v \in b_k$ for block b_k in partition Ψ , and local false-discovery rates require marginal poste-

rior probabilities. Integrating out inverse Wishart distributions over the covariance matrices is possible analytically. We find:

$$f(\mathbf{X}, \mathbf{Y} \mid \boldsymbol{\mu}_X, \boldsymbol{\mu}_Y, \boldsymbol{\Delta}, \Psi) = C \frac{|A|^{\frac{\text{df}}{2}} |B|^{\frac{\text{df}}{2}}}{|\tilde{A}|^{\frac{\text{df}+M_X}{2}} |\tilde{B}|^{\frac{\text{df}+M_Y}{2}}} \quad (2.3)$$

where

$$\begin{aligned} S_1 &= \frac{1}{M_X - 1} \sum_{m=1}^{M_X} (\mathbf{X}_m - \bar{\mathbf{X}})(\mathbf{X}_m - \bar{\mathbf{X}})^\tau, & S_2 &= (\bar{\mathbf{X}} - \boldsymbol{\mu}_X)(\bar{\mathbf{X}} - \boldsymbol{\mu}_X)^\tau \\ T_1 &= \frac{1}{M_Y - 1} \sum_{r=1}^{M_Y} (\mathbf{Y}_r - \bar{\mathbf{Y}})(\mathbf{Y}_r - \bar{\mathbf{Y}})^\tau, & T_2 &= (\bar{\mathbf{Y}} - \boldsymbol{\mu}_Y)(\bar{\mathbf{Y}} - \boldsymbol{\mu}_Y)^\tau \\ \tilde{A} &= A + (M_X - 1)S_1 + M_X S_2, & \tilde{B} &= B + (M_Y - 1)T_1 + M_Y T_2 \end{aligned}$$

and where C is a normalizing constant. In the above, $|\cdot|$ denotes matrix determinant, $\bar{\mathbf{X}} = \frac{1}{M_X} \sum_{m=1}^{M_X} \mathbf{X}_m$, $\bar{\mathbf{Y}} = \frac{1}{M_Y} \sum_{r=1}^{M_Y} \mathbf{Y}_r$, and S_1 and T_1 are sample covariance matrices of \mathbf{X} and \mathbf{Y} . In (2.3) there is conditional independence of data from the two conditions given the means but marginal to the unspecified covariance matrices. We use the Laplace approximation to numerically integrate the freely-varying means in order to obtain the marginal predictive density $f(\mathbf{X}, \mathbf{Y} \mid \boldsymbol{\Delta}, \Psi)$ (Supplementary Material, Equation 0.2).

By not constraining the sample covariance matrices U and V the GraphMM model does not adopt a product-partition form. In such, the predictive density would factor over blocks in the graph-respecting partition, and this would lead to simpler computations. We found in preliminary numerical experiments that various data sets are not consistent with this simplified dependence pattern, and we therefore propose the general form here. Per voxel computations remain relatively efficient since we work on small, local graphs.

2.3 Data-driven simulations

Our primary evaluation of GraphMM is through a set of simulations designed around a motivating data set from the Alzheimer's Disease Neuroimaging Initiative 2 (ADNI-2) (Section 2.4).

Briefly, we consider structural brain imaging data from a group of $M_X = 123$ normal control subjects (group 1) and a second group of $M_Y = 148$ subjects suffering from late-stage mild cognitive impairment (MCI), a precursor to Alzheimer’s disease (AD), and for the simulation we focus on a single coronal slice containing $N = 5236$ voxels. We cluster the empirical mean profiles to generate blocks for the synthetic expected values, and we use covariance matrices estimated from the replicate brain slices. Three synthetic data sets are generated in each simulation scenario. The first three scenarios address the issue of block size; the next two investigate the role of the distribution of condition effects. To assess robustness, we also consider parameter settings where partitions are not graph respecting, and condition effects are not uniform over blocks. Further, we deploy two permutation experiments; the first uses sample label permutation to confirm the control of the false-discovery rate, and the second uses voxel permutation to confirm that sensitivity drops when we disrupt the spatially coordinated signal.

When applying GraphMM to each synthetic data set, we estimate hyperparameters for all distributional components and consider discoveries as $\mathcal{L}(c) = \{v : l_v \leq c\}$ for various thresholds c . We call the controlled FDR the mean $\sum_v l_v 1[v \in \mathcal{L}(c)] / \sum_v 1[v \in \mathcal{L}(c)]$, as this is the conditional expected rate of type-1 errors on the list, given data (and computable from data). We know the null status in each synthetic case, and so we also call the empirical FDR to be that rate counting latent null indicators; likewise the true positive rate counts the non-null indicators. We compare GraphMM to several contemporary testing methods, including Benjamini-Hochberg correction (BH adj), Benjamini and Hochberg (1995), local FDR, (locfdr) Efron (2007), and q -value (qvalue), Storey (2003), that are all applied to voxel-specific t-tests. We also compare results to adaptive shrinkage, Stephens (2017), both the local FDR statistic (ash_lfdr) and the q -value (ash_qval). These methods do not leverage the graphical nature of the data, and all work on summaries of voxel-specific tests; summaries may be p-values (for BH and q-value), or t-statistics (for locFDR), or effect estimates and estimated standard errors (for ASH).

2.4 Brain MRI study

Gray matter tissue probability maps derived from the co-registered T1-weighted magnetic resonance imaging (MRI) data were pre-processed using the voxel-based morphometry (VBM) toolbox in Statistical Parametric Mapping software (SPM, <http://www.fil.ion.ucl.ac.uk/spm>). The ADNI-2 data includes 3D brain images of 148 cognitively normal control subjects and 123 subjects with late-stage mild cognitive impairment (MCI). Prior to registration to a common template, standard artifact removal and other corrections were performed, as described in Ithapu *and others* (2015). We filtered voxels having very low marginal standard deviation (Bourgon *and others*, 2010), leaving 464441 voxels, and then converted the data to rank-based normal scores.

3. RESULTS

3.1 Operating characteristics of GraphMM

Synthetic data sets mimic the structure and empirical characteristics of the brain MRI study data. The first three synthetic-data scenarios consider a single MRI brain slice measured on replicates from two conditions, with characteristics approximately matching the characteristics of observed data (Supplementary Material, Table S2). These scenarios vary the underlying size distribution of blocks, but follow the GraphMM model in the sense that the underlying signal has graph-respecting partitions, and other conditions such as block-level shifts between conditions and multivariate Gaussian errors are satisfied. The left panel of Fig. 3 shows that all methods on test are able to control the false-discovery rate. All methods display sensitivity for the signals, though GraphMM demonstrates superior power in the first two cases where blocks extend beyond the individual voxel. The high sensitivity in Scenario 2 may reflect that the prior distribution of block sizes used in the local GraphMM more closely matches the generative situation. Notably, even when this block-size distribution is not aligned with the GraphMM prior,

we do not see an inflation of the false-discovery rate.

Scenarios 4 and 5 are similar to the first cases, however they explore different forms of signals between the two groups; both have an average block size of 4 voxels, but in one case the changed block effects are fewer, relatively strong and in the other case they are more frequent, and relatively weaker (Supplementary Material, Table S3). In both regimes, GraphMM retains its control of FDR and exhibits good sensitivity compared to other methods (Fig. 4).

GraphMM is designed for the case where partition blocks are graph respecting and the changes between conditions affect entire blocks. Our next numerical experiment checks the robustness of GraphMM when this partition/change structure is violated Fig. 5 shows that GraphMM continues to control FDR and also retains a sensitivity advantage even when its underlying model is not fully correct.

To further assess the properties of GraphMM, we performed two permutation experiments leveraging the ADNI-2 data. In the first, we permuted the sample labels of the 148 control subjects and 123 late MCI subjects, repeating for ten permuted sets. On each permuted set, we applied various methods to detect differences. All discoveries are false discoveries in this null case. The left panel of Fig. 6 shows that GraphMM and other methods are correctly recognizing the apparent signals as being consistent with the null hypothesis. The second permutation experiment retains the sample-grouping information, but permutes the voxels within the brain slice on test. This permutation disrupts both spatial measurement dependencies and any spatial structure in the signal. Since GraphMM is leveraging spatially-coherent patterns in signal, we expect it to produce fewer statistically significant findings in this voxel-permutation case. The right panel of Fig. 6 shows this dampening of signal as we expect, when looking at the empirical cdf of computed values $l_v = P(H_{0,v}|X, Y)$.

3.2 ADNI-2 data analysis

Using data from ADNI-2 we seek to evaluate the sensitivity of GraphMM in identifying significant differences between two disease stages (cognitively normal controls and late MCI), and also assess the extent to which our findings are corroborated by known results on aging and Alzheimer’s disease. The methodology detects locations (i.e., voxels) where the distribution of MRI-based gray matter intensities is significantly different between control subjects and subjects with late MCI. To keep the computational burden manageable, we applied GraphMM to 2D image slices in the coronal direction, instead of processing the entire 3D image volume at once. For comparison, we applied Statistical non-parametric Mapping toolbox using Matlab, SnPM, which is a popular image analysis method used in neuroscience, and q -value with adaptive shrinkage using R, *ashr*, which represents an advanced voxel-specific empirical-Bayes method.

Fig. 7 shows a representative example output for a montage of 4 coronal slices extracted from the 3D image volume. The color bar (red to yellow), for each method presented, is a surrogate for the strength of some score describing the group-level difference: for instance, for SnPM, the color is scaled based on adjusted p -values, for the q -value method, it is scaled based on q -values, whereas for GraphMM, the color is scaled based on local false-discovery rates l_v . While the regions reported as significantly different between controls and late MCI have some overlap between the different methods, GraphMM is able to identify many more significantly different voxels compared to baseline methods, at various FDR thresholds (Supplementary Material, Fig. S4). A closer inspection of one case is informative (Fig. 8). Voxel v at coordinates ($x = 31, y = 53, z = 23$) is not found to be different between control and late MCI according to SnPM (adjusted p -value = 0.578) or the ASH q -value method (q -value = 0.138). But when we look at the results provided by GraphMM, the local FDR is 0.001. The increased sensitivity of GraphMM may come from its leveraging the consistent pattern of shifts among neighboring voxels.

A statistical measure often reported in the neuroimaging literature is the size of spatially connected sets of significantly altered voxels in the 3D lattice (so-called significant clusters). The rationale is that stray (salt and pepper) voxels reported as significantly different may be more likely to be an artifact compared to a group of anatomically clustered voxels. We find that GraphMM performs favorably relative to the baseline methods in that it consistently reports larger significant clusters (Supplementary Material, Fig. S5).

To provide some neuroscientific interpretation of the statistical findings, we use the Matlab package *xjview* to link anatomical information associated with significantly altered voxels (Tzourio-Mazoyer *and others*, 2002). Results for the top 15 brain regions are summarized in Table 1. We see that GraphMM discovers all the brain regions found by SnPM, with many more significant voxels in each region. The only exception is the hippocampus, where both methods identify a large number of voxels but GraphMM finds fewer significant voxels than SnPM. In addition, there are regions revealed to be significant by GraphMM but not by SnPM, including the precentral gyrus, middle frontal gyrus, inferior frontal gyrus opercular, insular, anterior cingulate, and supramarginal gyrus, which are relevant in the aging and AD literature. GraphMM consolidates known alterations between cognitively normal and late-stage MCI and reveals potentially important new findings.

4. DISCUSSION

Mass univariate testing is the dominant approach to detect statistically significant changes in comparative brain-imaging studies (e.g., Groppe *and others* (2011)). In such, a classical testing procedure, like the test of a contrast in a regression model, is applied in parallel over all testing units (voxels), leading to a large number of univariate test statistics and p-values. Subsequently, significant voxels are identified through some filter, such as the Benjamini-Hochberg (BH) procedure, that aims to control the false-discovery rate. The approach can be very effective and has

supported numerous important applied studies of brain function. In structural magnetic resonance image studies of Alzheimer’s disease progression, such mass univariate testing has failed in some cases to reveal subtle structural changes between phenotypically distinct patient populations. The underlying problem is limited statistical power for relatively small effects, even with possibly hundreds of subjects per group. Power may be recovered by empirical Bayes procedures that leverage various properties of the collection of tests. The proposed GraphMM method recognizes simplified parameter states when they exist among graphically related testing units. We deploy GraphMM locally in the system-defining graph by separately processing a small subgraph for each testing unit, while allowing hyper-parameters to be estimated globally from all testing units. Essentially we provide an explicit and flexible joint probability model for all data on each subgraph (Equation 2.3). The model entails a discrete parameter state on this subgraph, which describes how the nodes on the subgraph are partitioned into blocks, and whether or not each block is shifted between the two sampling conditions being compared. By deriving local FDR computations on a relatively small subgraph for each testing unit, we simplify computations and we share perhaps the most relevant information that is external to that testing unit. Numerical experiments confirm the control of FDR and the beneficial power properties of GraphMM, whether the model specification is valid or violated in various ways. The methodology also reveals potentially interesting brain regions that exhibit significantly different structure between normal subjects and those suffering mild cognitive impairment.

The Dirichlet process mixture (DPM) model also entails a clustering of the inference units, with units in the same cluster block if (and only if) they share the same parameter values. The DPM model has been effective at representing heterogeneity in a system of parameters (e.g., Muller and Quintana (2004)), and in improving sensitivity in large-scale testing (e.g., Dahl and Newton (2007), Dahl *and others* (2008)). Benefits typically come at a high computational cost, since in principle the posterior summaries require averaging over all partitions of the units

(e.g., Blei and Jordan (2006)). There are also modeling costs: DPM's usually have a product-partition form in which the likelihood function factors as a product over blocks of the partition (Hartigan (1990)). We observe that independence between blocks is violated in brain-image data in a way that may lead to inflation of the actual false-discovery rate over a target value.

Graphs have been widely used for modeling data arising in various fields of science. In the present work, vertices of the graph correspond to variables in a data set and the undirected edges convey relational information about the connected variables, due to associations with the context of the data set, such as temporal, functional, spatial, or anatomical information. The graphs we consider constitute an auxiliary part of observed data. For clarity, these graphs may or may not have anything to do with undirected graphical representations of the dependence in a joint distribution (e.g. Lauritzen (1996)), as in the graphical models literature. For us, the graph serves to constrain patterns in the expected values of measurements. By limiting changes in expected values over the graph, we aim to capture low complexity of the system. An alternative way to model low-complexity is through smoothed, bandlimited signals (e.g., Ortega *and others* (2018), Chen *and others* (2016)). Comparisons between the approaches are warranted. We have advanced the idea of latent graph-respecting partitions that constrain expected values into low-dimensional space. Figure S3 in the Supplementary Material investigates benefits of the graph-respecting assumption on posterior concentration, and supports the treatment of this constraint as having a regularizing effect. The partition is paired with a vector of block-specific change indicators to convey the discrete part of the modeling specification. We used a uniform distribution over graph-respecting partitions in our numerical experiments, and have also considered more generally the distribution found by conditioning a product partition model (PPM) to be graph-respecting. In either case, two vertices that are nearby on the graph are more likely to share expected values, in contrast to the exchangeability inherent in most partition models. Graph restriction greatly reduces the space of partitions; we enumerated all such partitions

in our proposed graph-local computations. When the generative situation is similarly graph restricted, we expect improved statistical properties; but we also showed that false-discovery rates are controlled even if the generative situation is not graph respecting. Special cases of graph-restricted partitions have been studied by others, including Page and Quintana (2016) for lattice graphs, Caron and Doucet (2009) for decomposable graphs, and Blei and Frazier (2011) for graphs based on distance metrics. When G is a complete graph there is no restriction and all partitions have positive mass. When G is a line graph the graph-respecting partition model matches Barry and Hartigan (1992) for change-point analysis.

ACKNOWLEDGEMENTS

This research was supported in part by NIH grant 1U54AI117924 to the University of Wisconsin Center for Predictive Computational Phenotyping. The authors were also supported in part by NIH R01 AG040396, NSF CAREER award RI 1252725, and NSF award 1740707 to the University of Wisconsin Institute for the Foundations of Data Science. We are grateful to Prof. Barbara Bendlin (Wisconsin ADRC, University of Wisconsin) for various discussions and in particular, for her help in evaluating the results on brain imaging data.

REFERENCES

- AMINOFF, ELISSA, KVERAGA, KESTUTIS AND BAR, MOSHE. (2013, 07). The role of the parahippocampal cortex in cognition. *Trends in cognitive sciences* **17**, 379–390.
- BARRY, DANIEL AND HARTIGAN, J. A. (1992, 03). Product partition models for change point problems. *Ann. Statist.* **20**(1), 260–279.
- BENJAMINI, YOAV AND HOCHBERG, YOSEF. (1995). Controlling the false discovery rate: A practical and powerful approach to multiple testing. *Journal of the Royal Statistical Society. Series B (Methodological)* **57**(1), 289–300.
- BIGLER, ERIN D., MORTENSEN, SHERSTIN, NEELEY, E. SHANNON, OZONOFF, SALLY, KRASNY, LORI, JOHNSON, MICHAEL, LU, JEFFREY, PROVENCAL, SHERRI L., McMAHON, WILLIAM AND LAINHART, JANET E. (2007). Superior temporal gyrus, language function, and autism. *Developmental Neuropsychology* **31**(2), 217–238. PMID: 17488217.
- BLEI, DAVID M. AND FRAZIER, PETER I. (2011, November). Distance dependent Chinese restaurant processes. *J. Mach. Learn. Res.* **12**, 2461–2488.

- BLEI, DAVID M. AND JORDAN, MICHAEL I. (2006, 03). Variational inference for Dirichlet process mixtures. *Bayesian Anal.* **1**(1), 121–143.
- BOURGON, RICHARD, GENTLEMAN, ROBERT AND HUBER, WOLFGANG. (2010, 05). Independent filtering increases detection power for high-throughput experiments. *Proceedings of the National Academy of Sciences of the United States of America* **107**, 9546–51.
- CARON, FRANÇOIS AND DOUCET, ARNAUD. (2009). Bayesian nonparametric models on decomposable graphs. In: *Proceedings of the 22Nd International Conference on Neural Information Processing Systems, NIPS'09*. USA: Curran Associates Inc. pp. 225–233.
- CHEN, S., VARMA, R., SINGH, A. AND KOVACEVIC, J. (2016). Signal recovery on graphs: Fundamental limits of sampling strategies. *IEEE Transactions on Signal and Information Processing over Networks* **2**(4), 539–554.
- COHEN, N. J. AND EICHENBAUM, H. (1993). *Memory, amnesia, and the hippocampal system*. MIT Press.
- DAHL, DAVID B, MO, QIANXING AND VANNUCCI, MARINA. (2008). Simultaneous inference for multiple testing and clustering via a Dirichlet process mixture model. *Statistical Modelling* **8**(1), 23–39.
- DAHL, DAVID B AND NEWTON, MICHAEL A. (2007). Multiple hypothesis testing by clustering treatment effects. *Journal of the American Statistical Association* **102**(478), 517–526.
- DO, KIM ANH, MÜLLER, PETER AND TANG, FENG. (2005). A Bayesian mixture model for differential gene expression. *Journal of the Royal Statistical Society. Series C: Applied Statistics* **54**(3), 627–644.
- EFRON, BRADLEY. (2007, 08). Size, power and false discovery rates. *Ann. Statist.* **35**(4), 1351–1377.
- EFRON, BRADLEY. (2010). *Large-Scale Inference: Empirical Bayes Methods for Estimation, Testing, and Prediction*, Institute of Mathematical Statistics Monographs. Cambridge University Press.
- EKLUND, ANDERS, NICHOLS, THOMAS E. AND KNUTSSON, HANS. (2016). Cluster failure: Why fmri inferences for spatial extent have inflated false-positive rates. *Proceedings of the National Academy of Sciences* **113**(28), 7900–7905.
- GENOVESE, CHRISTOPHER R., LAZAR, NICOLE A. AND NICHOLS, THOMAS. (2002). Thresholding of statistical maps in functional neuroimaging using the false discovery rate. *NeuroImage* **15**(4), 870 – 878.
- GOGOLLA, NADINE. (2017). The insular cortex. *Current Biology* **27**(12), R580 – R586.
- GRAHN, JESSICA A., PARKINSON, JOHN A. AND OWEN, ADRIAN M. (2008). The cognitive functions of the caudate nucleus. *Progress in Neurobiology* **86**(3), 141 – 155.
- GRAZIANO, MICHAEL S.A, TAYLOR, CHARLOTTE S.R AND MOORE, TIRIN. (2002). Complex movements evoked by microstimulation of precentral cortex. *Neuron* **34**(5), 841 – 851.
- GREENLEE, JEREMY D.W., OYA, HIROYUKI, KAWASAKI, HIROTO, VOLKOV, IGOR O., SEVERSON III, MERYL A., HOWARD III, MATTHEW A. AND BRUGGE, JOHN F. (2007). Functional connections within the human inferior frontal gyrus. *Journal of Comparative Neurology* **503**(4), 550–559.
- GROPPE, DAVID M., URBACH, THOMAS P. AND KUTAS, MARTA. (2011). Mass univariate analysis of event-related brain potentials/fields i: A critical tutorial review. *Psychophysiology* **48**(12), 1711–1725.
- HARTIGAN, J. A. (1990, 01). Partition models. *Communications in Statistics-theory and Methods* **19**, 2745–2756.
- HARTWIGSEN, GESA, BAUMGAERTNER, ANNETTE, PRICE, CATHY J, KOEHNKE, MARIA, ULMER, STEPHAN AND SIEBNER, HARTWIG R. (2010, September). Phonological decisions require both the left and right supra-marginal gyri. *Proceedings of the National Academy of Sciences of the United States of America* **107**(38), 16494—16499.

- ITHAPU, VAMSI K, SINGH, VIKAS, OKONKWO, OZIOMA C, CHAPPELL, RICHARD J, DOWLING, N MARITZA, JOHNSON, STERLING C, INITIATIVE, ALZHEIMER'S DISEASE NEUROIMAGING *and others*. (2015). Imaging-based enrichment criteria using deep learning algorithms for efficient clinical trials in mild cognitive impairment. *Alzheimer's & Dementia* **11**(12), 1489–1499.
- JAPEE, SHRUTI, HOLIDAY, KELSEY, SATYSHUR, MAUREEN D., MUKAI, IKUKO AND UNGERLEIDER, LESLIE G. (2015). A role of right middle frontal gyrus in reorienting of attention: a case study. *Frontiers in Systems Neuroscience* **9**, 23.
- KIM, SINA, B. DAHL, DAVID AND VANNUCCI, MARINA. (2009, 01). Spiked Dirichlet process prior for Bayesian multiple hypothesis testing in random effects models. *Bayesian Analysis* **4**, 707–732.
- KNAFO, SHIRA. (2012, 12). Amygdala in Alzheimer's disease. In: Ferry, Barbar (editor), *The Amygdala: A discrete multitasking manager*. BoD-Books on Demand.
- LAURITZEN, S.L. (1996). *Graphical Models*, Oxford Statistical Science Series. Clarendon Press.
- MARCHAND, WILLIAM, LEE, JAMES, W THATCHER, JOHN, W HSU, EDWARD, RASHKIN, ESTHER, SUCHY, YANA, CHELUNE, GORDON, STARR, JENNIFER AND STEADMAN BARBERA, SHARON. (2008, 06). Putamen coactivation during motor task execution. *Neuroreport* **19**, 957–60.
- MEADOWS, MARY-ELLEN. (2011). *Calcarine Cortex*. New York, NY: Springer New York, pp. 472–472.
- MOLLER, CHRISTIANE, VRENKEN, HUGO, JISKOOT, LIZE, VERSTEEG, ADRIAAN, BARKHOF, FREDERIK, SCHELTENS, PHILIP AND VAN DER FLIER, WIESJE M. (2013). Different patterns of gray matter atrophy in early- and late-onset Alzheimer's disease. *Neurobiology of Aging* **34**(8), 2014 – 2022.
- MULLER, PETER AND QUINTANA, FERNANDO A. (2004, 02). Nonparametric Bayesian data analysis. *Statistical Science* **19**(1), 95–110.
- NEWTON, MICHAEL A., NOUEIRY, AMINE O, SARKAR, DEEPAYAN AND AHLQUIST, PAUL. (2004). Detecting differential gene expression with a semiparametric hierarchical mixture method. *Biostatistics* **5** **2**, 155–76.
- NICHOLS, TOM. Statistical nonparametric mapping - a toolbox for spm. <http://niso.org/Software/SnPM13/>.
- NICHOLS, THOMAS E. (2012). Multiple testing corrections, nonparametric methods, and random field theory. *NeuroImage* **62**(2), 811 – 815. 20 YEARS OF fMRI.
- ONITSUKA, TOSHIKI, SHENTON, MARTHA E., SALISBURY, DEAN F., DICKEY, CHANDLEE C., KASAI, KIYOTO, TONER, SARAH K., FRUMIN, MELISSA, KIKINIS, RON, JOLESZ, FERENC A. AND MCCARLEY, ROBERT W. (2004). Middle and inferior temporal gyrus gray matter volume abnormalities in chronic schizophrenia: An mri study. *American Journal of Psychiatry* **161**(9), 1603–1611. PMID: 15337650.
- ORTEGA, ANTONIO, FROSSARD, PASCAL, KOVACEVIC, JELENA, MOURA, JOSE AND VANDERGHEYNST, PIERRE. (2018, 05). Graph signal processing: Overview, challenges, and applications. *Proceedings of the IEEE* **106**, 808–828.
- PAGE, GARRITT L. AND QUINTANA, FERNANDO A. (2016, 03). Spatial product partition models. *Bayesian Anal.* **11**(1), 265–298.
- PENNY, WILLIAM, FRISTON, KARL, ASHBURNER, JOHN, J. KIEBEL, S AND E. NICHOLS, T. (2007, 01). *Statistical Parametric Mapping: The Analysis of Functional Brain Images*.
- PLOTZKER, ALAN, OLSON, INGRID R. AND EZZYAT, YOUSSEF. (2007, 03). The Enigmatic temporal pole: a review of findings on social and emotional processing. *Brain* **130**(7), 1718–1731.

- STEPHENS, MATTHEW. (2017). False discovery rates: a new deal. *Biostatistics* **18**(2), 275–294.
- STEVENS, FRANCIS L., HURLEY, ROBIN A., TABER, KATHERINE H., HURLEY, ROBIN A., HAYMAN, L. ANNE AND TABER, KATHERINE H. (2011). Anterior cingulate cortex: Unique role in cognition and emotion. *The Journal of Neuropsychiatry and Clinical Neurosciences* **23**(2), 121–125. PMID: 21677237.
- STOREY, JOHN D. (2003, 12). The positive false discovery rate: a Bayesian interpretation and the q -value. *Ann. Statist.* **31**(6), 2013–2035.
- TANSEY, WESLEY, KOYEJO, OLUWASANMI, POLDRACK, RUSSELL A. AND SCOTT, JAMES G. (2018). False discovery rate smoothing. *Journal of the American Statistical Association* **113**(523), 1156–1171.
- TZOURIO-MAZOYER, N., LANDEAU, B., PAPANATHANASSIOU, D., CRIVELLO, F., ETARD, O., DELCROIX, N., MAZOYER, B. AND JOLIOT, M. (2002). Automated anatomical labeling of activations in spm using a macroscopic anatomical parcellation of the mni mri single-subject brain. *NeuroImage* **15**(1), 273 – 289.
- VEMURI, PRASHANTHI AND JACK, CLIFFORD R. (2010, Aug). Role of structural mri in Alzheimer’s disease. *Alzheimer’s Research & Therapy* **2**(4), 23.
- WEINER, KEVIN S. AND ZILLES, KARL. (2016-03). The anatomical and functional specialization of the fusiform gyrus. *Neuropsychologia* **83**, 48,62.
- WEINER, MICHAEL W AND VEITCH, DALLAS P. (2015). Introduction to special issue: overview of Alzheimer’s disease neuroimaging initiative. *Alzheimer’s & Dementia* **11**(7), 730–733.
- WORSLEY, KEITH J., TAYLOR, JONATHAN E., TOMAIUOLO, FRANCESCO AND LERCH, JASON. (2004). Unified univariate and multivariate random field theory. *NeuroImage* **23**, S189 – S195. Mathematics in Brain Imaging.

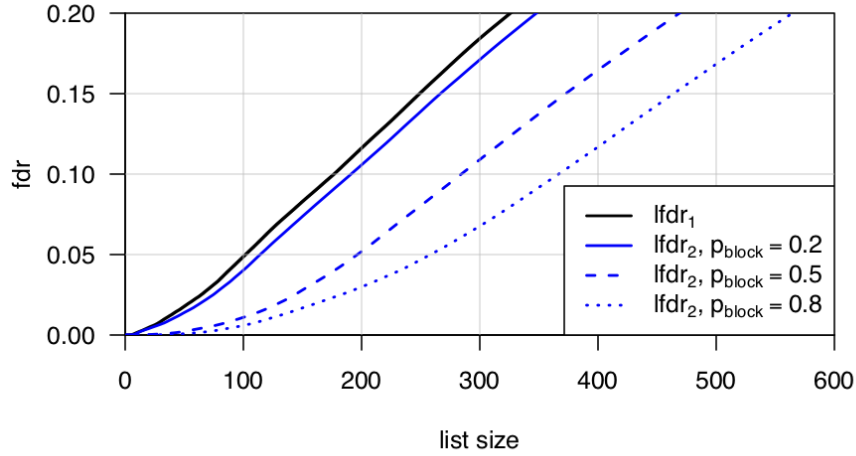


Fig. 1: False discovery rate (vertical) as a function of list size (horizontal) for various testing procedures. lfd_1 refers to the procedure to list the unit if the local false discovery rate $P(\mu_{X_1} = \mu_{Y_1} | X_1, Y_1)$ is sufficiently small (black). Blue lines refer to the operating characteristics when using lfd_2 which is $P(\mu_{X_1} = \mu_{Y_1} | X_1, X_2, Y_1, Y_2)$, for various probabilities p_{block} that the two units share parameters. By accounting for blocking, we benefit through increased yield for a given false-discovery-rate.

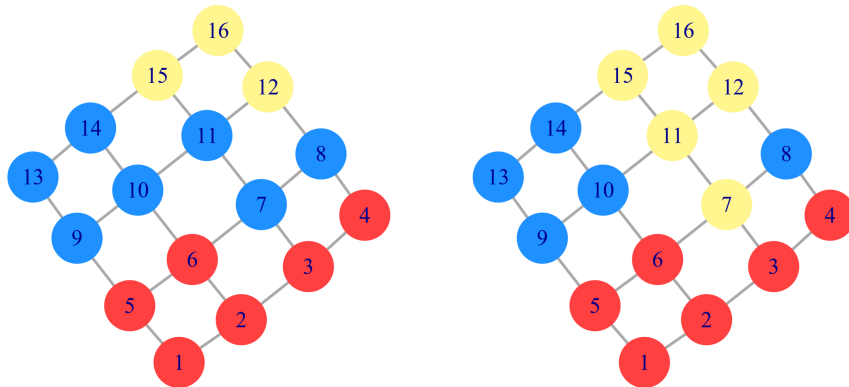


Fig. 2: Examples of partitions on a graph. Different colors represent different blocks. The partition on the left is graph-respecting while the one on the right is not (the blue block induces a subgraph with two components).

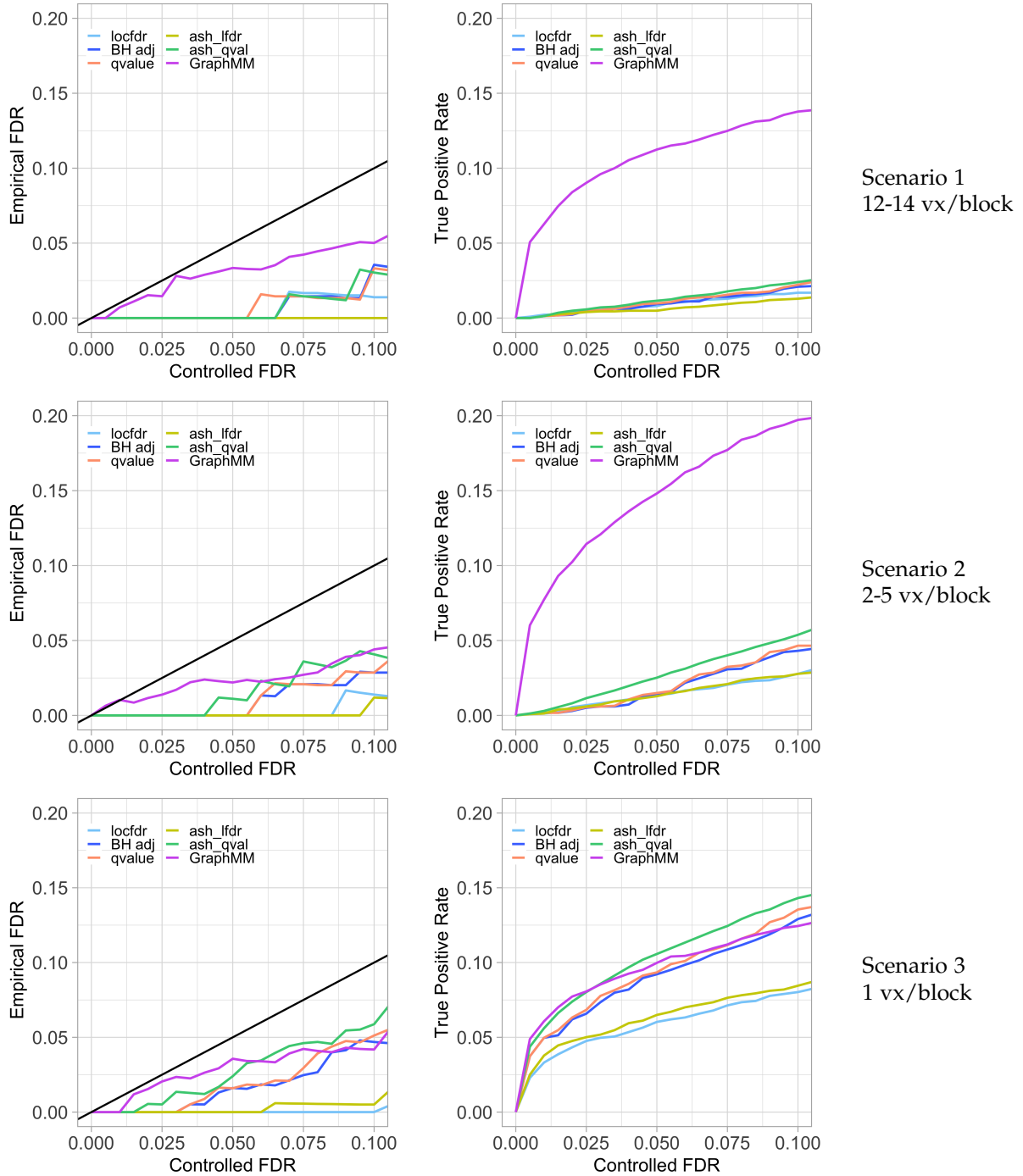


Fig. 3: Operating characteristics on synthetic data. Rows correspond to simulation scenarios (1=top, large blocks; 2=middle, small blocks; 3=bottom, tiny blocks). On the left we compare the empirical FDR with the target controlling FDR. Dominance by the diagonal (black) confirms that all methods are controlling FDR at the target rates. The right panels show how well different methods identify voxels that are truly different between the two groups. Substantial power gains are evident by GraphMM. Supplementary Table S1 provides simulation details.

Table 1: Brain regions with significant (5% FDR) change in gray matter volume found by GraphMM.

No.	Brain region	# Voxels		Neurological function
		GraphMM	SnPM	
1	Hippocampus	1411	1646	Receives and consolidates new memory about experienced events, allowing for establishment of long-term memories. [Cohen and Eichenbaum (1993)]
2	Parahippocampal Gyrus	1008	410	Involved in episodic memory and visuospatial processing [Aminoff <i>and others</i> (2013)].
3	Amygdala	710	365	Plays an essential role in the processing and memorizing of emotional reactions [Knafo (2012)]
4	Temporal Gyrus (superior, middle and inferior)	2031	287	Involved in various cognitive processes, including language and semantic memory processing (middle) as well as visual perception (inferior) and sound processing (superior) [Onitsuka <i>and others</i> (2004), Bigler <i>and others</i> (2007)]
5	Putamen	793	12	Linked to various types of motor behaviors, including motor planning, learning, and execution.[Marchand <i>and others</i> (2008)].
6	Fusiform Gyrus	735	308	Influence various neurological phenomena including face perception, object recognition, and reading [Weiner and Zilles (6 03)].
7	Temporal Pole (superior, middle)	882	74	Involved with multimodal analysis, especially in social and emotional processing. [Plotzker <i>and others</i> (2007)].
8	Precentral Gyrus	829	0	Consists of primary motor area, controlling body's movements. [Graziano <i>and others</i> (2002)].
9	Middle Frontal Gyrus	635	0	Plays essential role in attentional reorienting. [Japee <i>and others</i> (2015)].
10	Inferior Frontal Gyrus Opercular	573	0	Linked to language processing and speech production. [Greenlee <i>and others</i> (2007)].
11	Calcarine	381	22	Where the primary visual cortex is concentrated, processes visual information. [Meadows (2011)].
12	Caudate	437	46	Plays essential roles in motor processes and a variety of executive, goal-directed behaviours [Grahn <i>and others</i> (2008)].
13	Insular	275	0	Involved in consciousness, emotion and the regulation of the body's homeostasis [Gogolla (2017)].
14	Anterior Cingulate	260	0	Plays a major role in mediating cognitive influences on emotion. [Stevens <i>and others</i> (2011)].
15	Supramarginal Gyrus	225	0	Linked to phonological processing and emotional responses. [Hartwigsen <i>and others</i> (2010)].

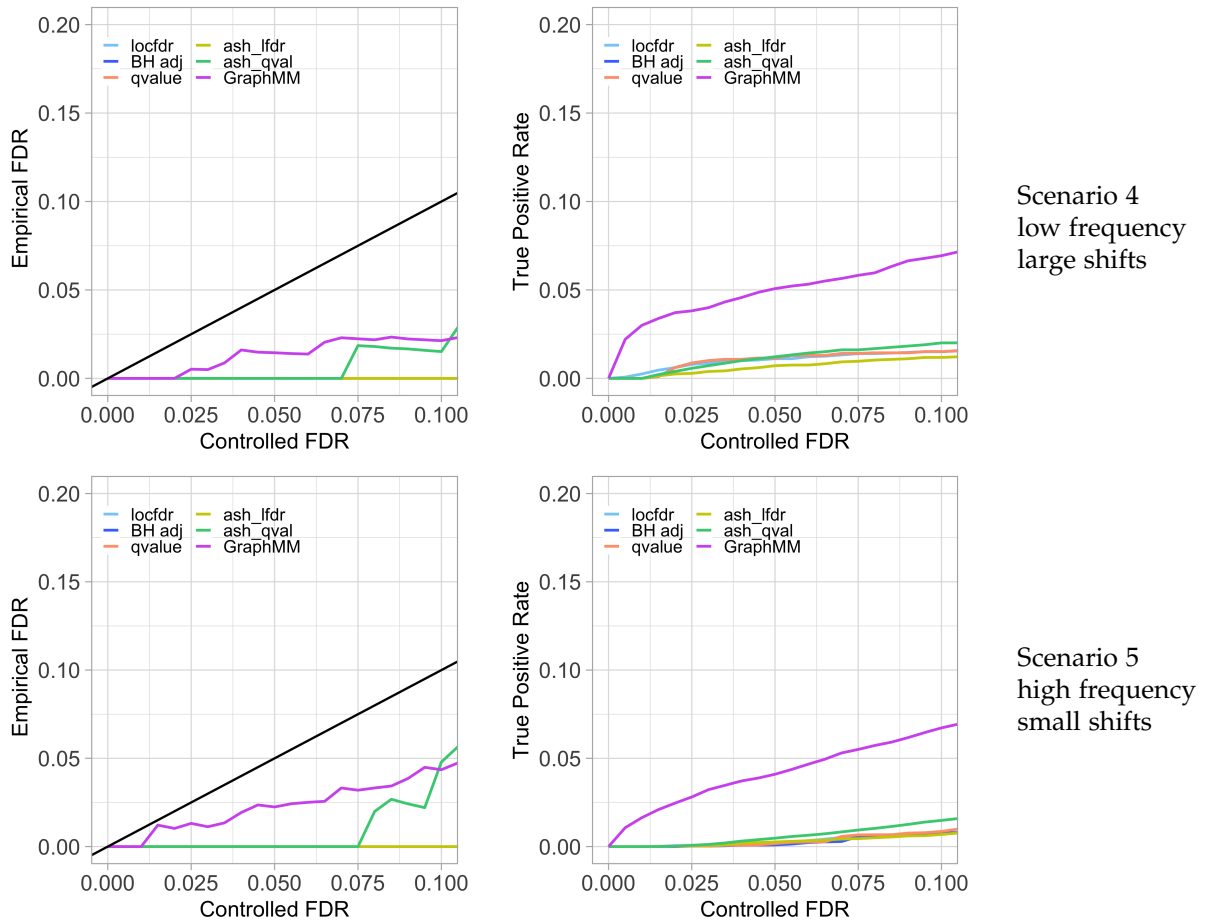


Fig. 4: Operating characteristics on synthetic data which explore different distributions of effects (Scenarios 4 and 5). Supplementary Table S2 has details.

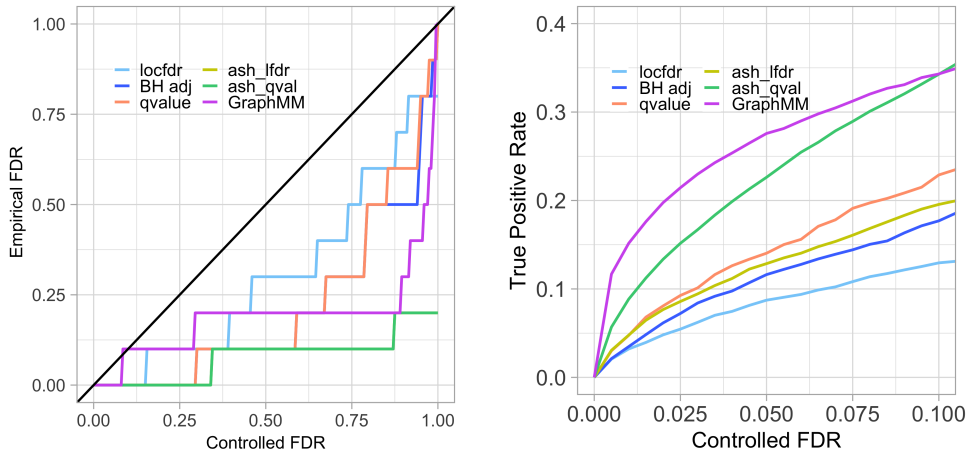


Fig. 5: Robustness to graph-respecting assumption. FDR (left) and sensitivity (right) in a case where latent partitions are not graph respecting, but have similarity 0.48 (Rand index).

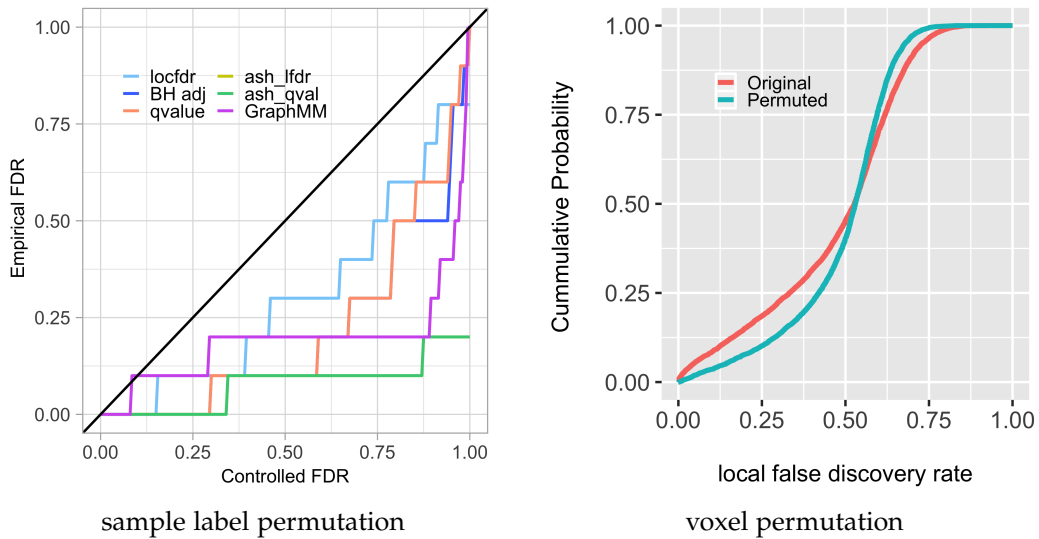


Fig. 6: Permutation experiments: The sample-label-permutation experiment confirms that GraphMM controls FDR in this no-signal case. The voxel-permutation experiment confirms that the detection rate is reduced when we disrupt the spatial signal.

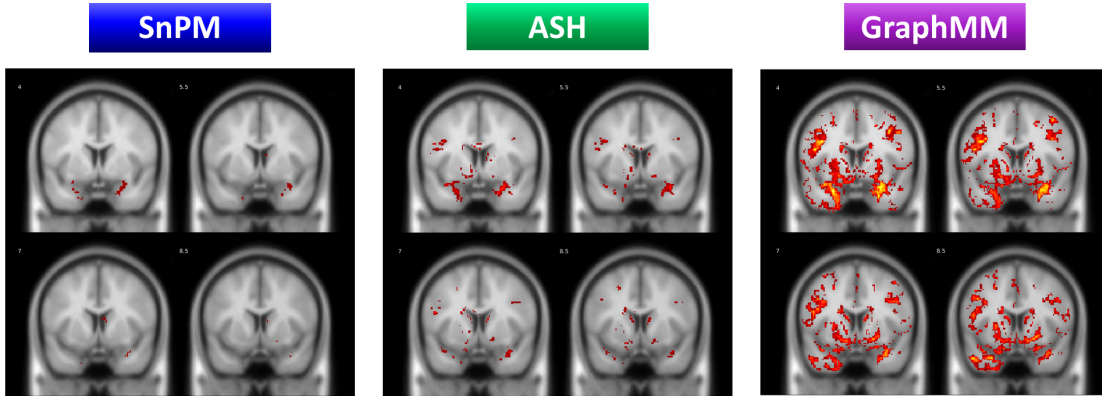


Fig. 7: Figure shows significantly different voxels at 5% FDR (colored area) for 4 coronal slices, found by Statistical non-parametric mapping (SnPM), adaptive shrinkage (ASH) and the proposed GraphMM.

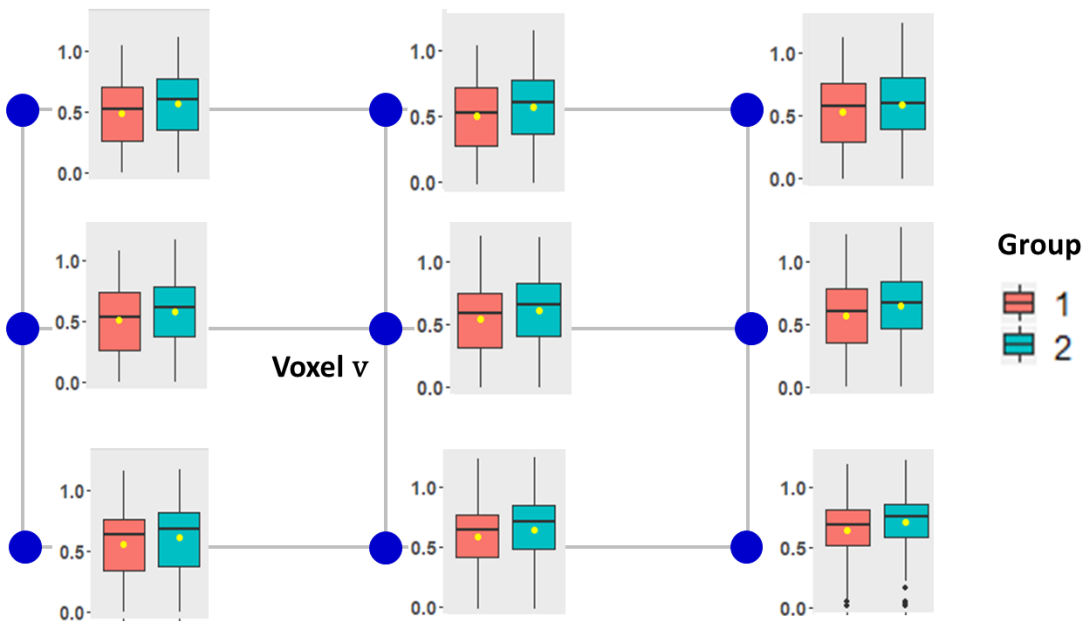


Fig. 8: Boxplots for voxel v at coordinates $(x = 31, y = 53, z = 23)$ and its neighbors. Voxel v is altered according to GraphMM but not according to SnPM or q -value. Similar shifts nearby v lead to the increased evidence reported by GraphMM.